

MIT Open Access Articles

*The TESS Faint-star Search: 1617
TOIs from the TESS Primary Mission*

The MIT Faculty has made this article openly available. **Please share** how this access benefits you. Your story matters.

Citation: Kunimoto, Michelle, Daylan, Tansu, Guerrero, Natalia, Fong, William, Bryson, Steve et al. 2022. "The TESS Faint-star Search: 1617 TOIs from the TESS Primary Mission." The Astrophysical Journal Supplement Series, 259 (2).

As Published: 10.3847/1538-4365/ac5688

Publisher: American Astronomical Society

Persistent URL: <https://hdl.handle.net/1721.1/142259>

Version: Final published version: final published article, as it appeared in a journal, conference proceedings, or other formally published context

Terms of use: Creative Commons Attribution 4.0 International License





The TESS Faint-star Search: 1617 TOIs from the TESS Primary Mission

Michelle Kunitomo¹ , Tansu Daylan^{1,2} , Natalia Guerrero³ , William Fong¹ , Steve Bryson⁴ , George R. Ricker¹ ,
Michael Fausnaugh¹ , Chelsea X. Huang^{1,5} , Lizhou Sha¹ , Avi Shporer¹ , Andrew Vanderburg¹ ,
Roland K. Vanderspek¹ , and Liang Yu¹

¹Department of Physics and Kavli Institute for Astrophysics and Space Research, Massachusetts Institute of Technology, Cambridge, MA 02139, USA
mkuni@mit.edu

²Department of Astrophysical Sciences, Princeton University, 4 Ivy Lane, Princeton, NJ 08544, USA

³Department of Astronomy, University of Florida, Gainesville, FL 32611, USA

⁴NASA Ames Research Center, Moffett Field, CA 94035, USA

Received 2021 December 3; revised 2022 February 8; accepted 2022 February 12; published 2022 March 14

Abstract

We present the detection of 1617 new transiting-planet candidates, identified in the Transiting Exoplanet Survey Satellite (TESS) full-frame images observed during the Primary Mission (Sectors 1–26). These candidates were initially detected by the Quick-Look Pipeline (QLP), which extracts full-frame image lightcurves for, and searches all stars brighter than, TESS magnitude $T = 13.5$ mag in each sector. However, QLP heavily relies on manual inspection for the identification of planet candidates, limiting vetting efforts to planet-hosting stars brighter than $T = 10.5$ mag and leaving millions of potential transit signals unvetted. We describe an independent vetting pipeline applied to QLP transit search results, incorporating both automated vetting tests and manual inspection to identify promising planet candidates around these fainter stars. The new candidates discovered by this ongoing project will allow TESS to significantly improve the statistical power of demographic studies of giant, close-in exoplanets.

Unified Astronomy Thesaurus concepts: [Exoplanets \(498\)](#); [Exoplanet detection methods \(489\)](#); [Transit photometry \(1709\)](#); [Time series analysis \(1916\)](#)

Supporting material: machine-readable table

1. Introduction

NASA’s Transiting Exoplanet Survey Satellite (TESS; Ricker et al. 2014) is the first nearly all-sky space-based transit search mission. Launched in 2018 April, its Primary Mission observed $\sim 73\%$ of the sky across 26 sectors, each lasting 27.4 days and covering a $24^\circ \times 96^\circ$ field of view. Observations were taken with two data collection modes: 2 minute sampled “postage stamps” image cutouts centered on $\sim 20,000$ pre-selected targets per sector, and 30 minute sampled full-frame images (FFIs) covering the entire TESS field of view. By the end of this two-year mission, TESS identified 2241 exoplanet candidates (Guerrero et al. 2021), known as TESS Objects of Interest (TOIs).

A major pipeline for the search and analysis of planet candidates in TESS FFIs is the Quick-Look Pipeline (QLP; Huang et al. 2020; Kunitomo et al. 2021) at the TESS Science Office at MIT. QLP performs multiaperture photometry to extract lightcurves for all targets with TESS magnitude $T < 13.5$ mag from TESS FFIs. At the end of each sector, all available data for targets observed in that sector are stitched together, and a box-least squares (BLS) transit search (Kovács et al. 2002) implemented in *vartools* (Hartman & Bakos 2016) is run on these multisector lightcurves. Following BLS, QLP applies basic detection criteria to identify transit candidates: at least 5 points in transit, a signal-to-noise

ratio of at least 9, and a signal-to-noise ratio (S/N) of at least 5 (if $T < 12$ mag) or 9 (otherwise).

QLP then performs automated triage for signals passing these detection criteria that orbit around stars with $T < 10.5$ mag using AstroNet-Triage (D. Moldovan et al. 2022, in preparation; Yu et al. 2019), a neural network for distinguishing eclipsing or transiting objects from noise, intrinsic stellar variability, and contact binary stars. QLP operators manually review candidates passing AstroNet (typically a few hundred per sector), produce vetting reports, and deliver the reports to TOI vetters for further inspection. Candidates passing group vetting are alerted as new TOIs on the TOI Release Portal.⁶

The QLP team’s choice to inspect signals only around stars brighter than $T = 10.5$ mag is primarily motivated by the fact that fainter searches would overwhelm operators and vetters with the number of candidates needing manual review. Indeed, over the entire Primary Mission, we found that 14,849,252 unique stars were searched and 2,507,460 BLS signals passed QLP’s detection criteria. We ran the AstroNet-Triage network used by QLP on these signals and identified 686,242 transit candidates that would nominally have needed manual inspection had the vetting magnitude limit been $T = 13.5$ mag.

In this paper, we describe our development of an additional, automated pipeline for QLP threshold-crossing events, and our subsequent use of this pipeline to vet the full sample of 682,242 signals passing AstroNet-Triage. This pipeline was largely inspired by the Robovetter, a fully automated vetting tool first used to compile Kepler’s DR24 catalog (Coughlin et al. 2016) and again for DR25 (Thompson et al. 2018). We also describe the final stage of manual vetting which resulted in the identification of over 1000 new faint-star TOIs.

⁵ Juan Carlos Torres Fellow.



Original content from this work may be used under the terms of the [Creative Commons Attribution 4.0 licence](#). Any further distribution of this work must maintain attribution to the author(s) and the title of the work, journal citation and DOI.

⁶ <https://tev.mit.edu/data/>

2. Identification of Planet Candidates

2.1. Automated Vetting

As mentioned in Section 1, QLP performs a multisector search of each target at the end of every sector. This means that a target observed in multiple sectors can correspond to several passing BLS signals, each from a different multisector search. We vet each BLS signal using the same QLP lightcurve that resulted in its detection.

Given that our vetting pipeline is not yet fully automated, our candidacy test thresholds were chosen empirically with the main purpose of reducing the number of signals needing manual inspection.

For any tests that required host-star properties as an input, we adopted those properties from the TESS Input Catalog (TIC) v8.1 (Stassun et al. 2019). We assumed solar values when stellar properties were not available.

2.1.1. Sine Wave Identification

BLS searches are often confounded by stellar variability with strong quasiperiodic and sinusoidal components over short timescales. Some eclipsing binaries may also feature strong ellipsoidal variations in the lightcurves. To identify these cases, we fit a sine wave to the lightcurve with periods fixed to half, exactly, and twice the BLS period using the nonlinear least-squares fitting package *lmfit* (Newville et al. 2016), letting the amplitude and phase of the sine wave vary. We quantified the significance of the fit by dividing the fitted amplitude by the uncertainty in the amplitude, and rejected any candidates with more than 15σ significance.

Due to there being more computationally expensive tests elsewhere in the pipeline, we ran the Sine Wave Identification test alone as the first step of automated vetting. A total of 212,967 (31% of all vetted signals) failed this test.

2.1.2. Model-shift Uniqueness Test

We employed the suite of model-shift uniqueness tests described in Coughlin (2017) to do the bulk of automated vetting on the remaining 469,275 signals. In summary, model-shift uses a transit model as a template to measure the amplitude of transit-like events at all phases in the phase-folded lightcurve. The procedure measures the significance and phases of the primary transit event, secondary and tertiary events, and the most significant positive flux (inverted transit-like) event. Model-shift also provides metrics such as the significance in the difference between odd and even transit events, and thresholds for determining if an event is significant compared to the noise level of the lightcurve. Overall, model-shift allows for the identification of false positives due to noise and systematics (identified as signals that are not unique compared to other events in the lightcurve, or with non-transit-like shapes), and those of astrophysical origin (identified as signals with significant secondary events or odd versus even depth differences).

Model-shift has been used in several automated vetting pipelines, including the Kepler Robovetter, the discovery and vetting of exoplanets tool designed for K2 (Kostov et al. 2019), and the TESS-ExoClass detection filter⁷ used to vet TESS candidates in the TESS Science Processing Operations Center

(SPOC; Jenkins et al. 2016) pipeline. To determine which candidates passed each test, we used the metric thresholds suggested in Coughlin (2017), although we recognize that these thresholds were designed to vet against typical Kepler systematics and should thus be considered suboptimal for TESS uses. We plan to tune these metric thresholds for a more TESS-specific automated vetting pipeline and possibly develop new, TESS-specific, metrics in the future.

Model-shift requires a transit model fit to the lightcurve as an input. We fit a Mandel & Agol (2002) quadratic limb-darkening transit model for each candidate,⁸ parameterized by the orbital period (P), transit epoch (T_0), ratio of planet-to-star radii (R_p/R_s), distance between planet and star at midtransit in units of stellar radius (a/R_s), and impact parameter (b), with circular orbits assumed. Limb-darkening parameters were taken from Claret (2017) based on stellar parameters from the TICv8.1 stellar catalog (Stassun et al. 2019). To speed up the fit process, data more than two transit durations from the BLS-inferred center of each transit were ignored.

We found that only 63,303 signals (13.4% of the $\sim 470,000$ signals) failed at least one test intended to identify systematics and other non-transit-like events (i.e., model-shift indicated that the primary transit event was not unique compared to other events in the lightcurve, the mean and median of transit depths were inconsistent, the transit was not a consistent decrease in flux as expected for a planet, and/or the shape of the transit was asymmetric). This is in line with expectations, given most non-transit-like signals among the BLS sample would have already been flagged by AstroNet-Triage, leaving astrophysical false positives as the most likely nonplanetary explanations. In turn, the model-shift tests against eclipsing binaries failed significantly more signals, with 95,203 (20.3%) signals failing to pass the model-shift thresholds based on significant odd versus even transit depths and 241,578 (50.4%) failing due to significant secondary events in the lightcurve. Overall, 363,618 (77.5%) signals failed at least one model-shift test.

2.1.3. Candidate Too Large

An indicator of an eclipsing binary (EB) false positive is an extremely deep eclipse, which implies that the radius of the eclipsing object is too large to be planetary. We multiplied the R_p/R_s fit results by the stellar radius of the target star and failed candidates with $R_p > 30R_\oplus$. We found that this test had the most significant discrimination power of any individual test, with 393,188 (83.8% of the 469,275 vetted signals) failing this test alone.

2.1.4. V-shape Test

While some EBs can be readily identified by their significant secondaries or large sizes, sufficiently grazing EBs ($b \gtrsim 1$) can have shallow eclipse depths that appear transit-like. These EBs can still be identified by both the depths and shapes of their eclipses. We adopted the Kepler DR25 Robovetter V-shape metric (Thompson et al. 2018), which required passing candidates have $R_p/R_s + b < 1.04$. We slightly relaxed this requirement to $R_p/R_s + b < 1.1$ to avoid inadvertently failing high-impact-parameter gas giants, especially those transiting small stars. Overall, 208,974 (44.5%) signals failed this test.

⁷ <https://github.com/christopherburke/TESS-ExoClass>

⁸ Adapted from <https://www.lpl.arizona.edu/~ianc/python/>.

2.1.5. Depth–Aperture Correlation

QLP produces multiple lightcurves for each star, extracted via circular aperture photometry using different radii. Larger apertures are appropriate for brighter targets in order to capture most of their flux. However, larger apertures also include more flux from nearby stars. This flux contamination can result in false positives from nearby eclipsing binaries (NEBs), whose deep eclipses can appear transit-like in the target’s lightcurve. An indication of NEB contamination is an increase in transit depth with aperture size.

We compared the lightcurves from Apertures 1 (radius of 2.5 pixels), 2 (3.0 pixels), and 3 (3.5 pixels) from QLP, where Aperture 1 is the default choice for the faintest stars ($T < 11.5$ mag) and Aperture 2 is the default choice for most brighter stars ($8.5 < T < 11.5$ mag). We measured the transit depths as the mean of the central 30 minutes of each phase-folded lightcurve, and estimated the noise by 1.4826 times the median absolute deviation of the out-of-transit lightcurve. 1.4826 is a conversion factor to put the variability on the same scale as a Gaussian standard deviation. We failed a candidate if an increase in aperture size resulted in a more than 1σ increase in transit depth. While this is a strict threshold, this was the only flux-level test capable of removing off-target signals, and we found that even small aperture–depth differences were reliable indicators of centroid offsets. This test flagged 186,124 (40.0%) signals as being likely off target due to depth–aperture correlation.

2.1.6. Centroid Offsets

The depth–aperture correlation test can identify NEBs that are well separated from the target, but pixel-level analysis is needed for closer contaminants. A powerful method for the identification of NEBs is the difference image technique described in Bryson et al. (2013). In summary, the average of in- and out-of-transit pixels surrounding the target are found from a candidate’s transit ephemerides and duration. The out-of-transit image represents a direct image of the field surrounding the target star. Meanwhile, the difference between the in- and out-of-transit images should appear starlike at the location of the transit source, assuming the transit is the explanation for any difference in flux. If the field is relatively uncrowded and the target star is indeed the source of the transit signal, the direct and difference images should appear similar.

We generated difference images using TESS-plots⁹, which includes a tool for difference image generation for candidates in TESS FFIs following the technique outlined in Bryson et al. (2013). Due to the computational expense of making and storing these data products, we only produced difference images for the 37,022 signals passing all previous tests. We also employed a simple, fast method to locate the source of the transit as the flux-weighted centroid of the difference image, calculated using center of mass from `scipy.ndimage` (Virtanen et al. 2020). We failed candidates for which the centroid was more than 1 pixel offset from the pixel location of the target star as predicted by the `tess-point`¹⁰ high-precision pointing tool (Burke et al. 2020). TESS-point uses the preplanned spacecraft pointings to predict the positions of targets on the detectors, and has a stated

precision of better than 1 pixel (smaller than our offset tolerance) when correcting for velocity aberration effects.

2.2. Manual Vetting

6936 signals passed the automated vetting pipeline and moved to manual vetting. Some of these signals corresponded to the same planet candidate reobserved over later sectors, leaving 5761 unique candidates. We produced vetting report pages to aid in the visual inspection of each unique candidate using all Primary Mission data available. An example report is shown for the 10.4 days planet candidate orbiting TIC-394346647 (now TOI-2620) in Figure 1, which is a $T = 12.99$ mag star observed in the Primary Mission during Sectors 1, 12, and 13. The vetting report includes plots of the full raw and detrended lightcurves from its three observed sectors, phase diagrams centered on the transit, odd versus even transits, the most significant secondary, and the transit in three different apertures. The report also includes the direct and difference images for by-eye identification of centroid offsets, and a list of relevant transit, planet, and stellar properties.

Two vetters independently reviewed each report that did not correspond to an already known TOI, and assigned either P (planet), F (false positive), or U (undecided) labels. Disagreements between vetters were discussed and resolved in group vetting sessions. Common candidates that needed to be resolved were those in crowded fields. One issue with high levels of crowding is an increased probability of NEB contamination, although manual inspection of the depth–aperture correlation and difference image plots were useful in identifying these cases. However, crowding can also cause transit-depth dilution, meaning our planet radii would be underestimated. Because many of the candidates we reviewed were giants, for which modest levels of dilution could increase their radii to nonplanetary values, we tended to treat candidates critically in crowded fields.

We also discussed candidates that may have been found with the wrong orbital period. These included strong single transits (which naturally have unknown periods), and those where the BLS search had been affected by other events (such as a deep eclipse from an NEB). We critically evaluated these on a case-by-case basis, and in some cases remade our reports or recalculated the metrics with the revised ephemerides for further review.

A QLP operator produced standard QLP reports for all candidates labeled with P, with the inclusion of any available TESS Extended Mission data for targets that had been reobserved since the Primary Mission. Each QLP report was then reviewed by the operator as a final manual check that the signal was still consistent with a planet interpretation before delivering the candidates to the TOI release portal, from which they were alerted as a TOI. Some of our candidates had Extended Mission data available at the time of QLP report production and were subsequently determined to no longer be consistent with a planet interpretation. In these cases, the additional data points at the improved 10 minute cadence of the Extended Mission FFIs helped to distinguish previously unclear odd versus even transit-depth differences and significant secondary events in the lightcurve. Our future faint-star analysis on Extended Mission FFIs will assess the additional discriminatory power of the 10 minute cadence data on our pipeline.

⁹ <https://github.com/mkunimoto/TESS-plots>

¹⁰ <https://github.com/christopherburke/tess-point>

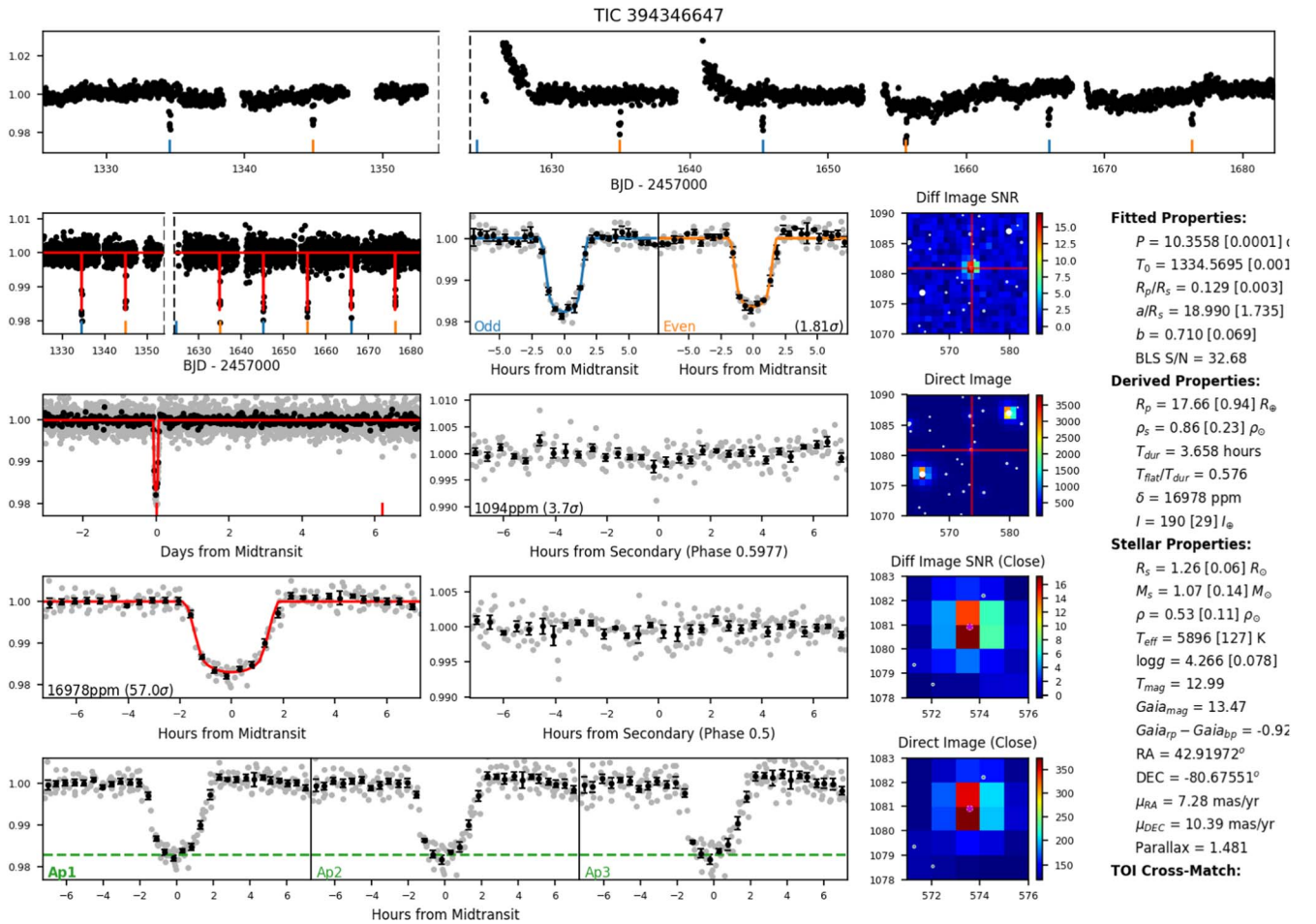


Figure 1. The vetting page for the 10.4 days planet candidate orbiting TIC-394346647 (now TOI-2620), containing data across Sectors 1, 12, and 13. Top row: raw lightcurve, with odd and even transits marked in blue and orange, respectively. Second row, first panel: detrended lightcurve with the transit model in red. Second row, second panel: odd and even transit phase diagrams. Third row, first panel: full phase diagram. Third row, second panel: phase diagram zoomed into the most significant secondary event from model-shift. Fourth row, first panel: phase diagram close-up to a transit event with the transit model in red. Fourth row, second panel: phase diagram close-up to phase 0.5. Fifth row: phase diagram close-up to a transit event in three different apertures. Second-last column: Full 20×20 pixel view of difference and direct images for Sector 13, followed by a close-up of the central 5×5 pixels. The target star is marked by a pink star. Nearby stars down to 4 mag fainter are plotted with circles. Last column: fitted and derived parameters from the transit model, BLS, and TIC, and the stellar catalog, with an indication of any matches to known TOIs.

Nine of the faint-star TOI hosts had been observed with 2 minute cadence observations during the TENN Primary Mission.¹¹ We checked each of these targets for NPOC threshold-crossing events (TCEs)¹², finding that six of the nine stars did not result in TCEs. All of these candidates had low S/N or only one to two transits per sector. We believe that these candidates went undetected by the SPOC pipeline primarily because fewer sectors of 2 minute data were available for SPOC than sectors of FFI data were available for QLP.

Two of the remaining three hosts had SPOC TCEs which failed the data validation (DV) stage of the SPOC pipeline, though the TCEs did not match our planet candidates. TIC-229786610 gave a non-transit-like $P = 0.27$ day TCE signal in SPOC multisector, whereas QLP revealed a $P = 22.2$ day, $S/N = 10$ candidate later alerted as TOI-4113.01. TIC-169461816 also gave a non-transit-like $P = 0.27$ day SPOC TCE in both single- and multi-sector searches, whereas QLP detected a single transit at $T_0 = 2,458,729.2$ days (BJD). This candidate was later alerted as

TOI-3563.01, and is an independent TESS detection of the known planet Kepler-448 c ($P = 17.9$ days, $T_0 = 2,454,979.6$ days).

Finally, one faint-star TOI matched an SPOC detection that passed DV. TIC-301160638 (TOI-3487) revealed the same two-transit, $P = 16.0$ days signal in both SPOC and QLP data. Vettters likely failed the signal from the SPOC report due to a deep event ~ 6 days after the first transit, which could indicate that the transits of TOI-3487.01 are secondaries of an eccentric eclipsing binary star. However, this event landed in data flagged as poor quality by QLP, and the out-of-transit flux surrounding the event in SPOC data is not flat. There were also not enough TESS observations to confirm that the event repeated. Because all other indications from both SPOC and QLP showed that TOI-3487.01 was consistent with a high S/N, on-target planet candidate, we opted to alert the signal.

3. Results and Discussion

A total of 1617 TOIs were alerted from the faint-star search, having started from the BLS results for 14.8 million stars observed over the TESS Primary Mission and searched by QLP. Faint-star TOIs are tracked in the TOI catalog by the

¹¹ <https://tess.mit.edu/observations/target-lists/>

¹² https://archive.stsci.edu/tess/bulk_downloads/bulk_downloads_tce.html

Table 1
The 1617 TOIs Alerted from this Work, Taken from the TOI Catalog (accessed 2022 January 24 from ExoFOP 2019)

TOI	TIC ID	TESS (mag)	R.A. (J2015.5)	Decl. (J2015.5)	Radius (R_{\oplus})	Period (days)	Epoch (BJD)	Depth (ppm)	Duration (hr)	Insolation (S_{\oplus})	Flags
2486.01	369376388	11.187	03:59:24.52	-36:28:33.69	3.73	1.5412	2,459,144.5382	1550	1.84	324.9	000
2492.01	282498590	11.675	06:00:23.94	05:06:52.09	17.90	10.1011	2,459,202.0540	13100	5.21	352.9	000
2500.01	206785987	11.619	06:26:47.75	08:12:03.52	13.91	2.9556	2,459,202.3112	7268	3.22	3422.7	000
2501.01	134471108	11.675	07:12:15.98	-44:01:39.16	2.90	5.3256	2,459,203.6552	1813	2.17	40.1	000
2531.01	262843259	12.433	03:30:07.49	-60:52:32.24	10.68	8.1484	2,459,156.0649	14290	3.19	90.5	000
2611.01	234282389	13.529	22:21:04.39	-64:42:44.17	5.16	0.7320	2,458,352.4849	4520	2.58	8999.6	000
2612.01	149572298	13.230	05:45:46.01	-61:39:36.08	19.30	13.3572	2,459,379.0181	29950	4.95	158.6	010
2613.01	52315301	13.149	01:31:38.54	-67:36:35.67	21.22	15.2015	2,459,075.8995	37010	8.33	266.2	000
2614.01	263075864	11.457	01:08:46.87	-78:10:23.23	14.97	4.8103	2,459,037.5892	21199	3.27	321.2	010
2615.01	38965512	13.205	00:45:54.66	-66:50:00.59	12.78	2.2688	2,459,112.5480	6270	2.79	1150.0	000

Note. The “Flags” column indicates if a TOI had a given host-star property available in the TIC Catalog (flag = 0), or if such values were missing and solar values were assumed (flag = 1). The column provides the flags for stellar radius, mass, and effective temperature, respectively.

(This table is available in its entirety in machine-readable form.)

comment “found in faint-star QLP search.” These TOIs and their properties are listed in Table 1. We also include a flag that indicates if their host stars had solar values assumed due to missing stellar properties from the TIC, indicating that 379 TOIs have some combination of missing stellar radius, mass, and/or effective temperature

3.1. Comparisons with Other TOIs

Figure 2 shows how the faint-star TOIs compare with other Primary Mission TOIs across period and radius space, with properties adopted from the TOI Catalog.¹³ The faint-star TOIs are clearly dominated by giant-planet candidates and those with short orbital periods. On average, the faint-star TOIs have orbital periods 21% shorter than other TOIs and 24% larger transit duty cycles. The giant, close-in planet bias has two explanations: First, lightcurve precision worsens as one moves to fainter stars, with noise on transit timescales on the order of 1000 ppm at $T \approx 13.5$ mag (Huang et al. 2020). Planet transits must therefore be very deep (several thousand parts per million) to be detectable around these faint stars, which naturally favors the detection of large planets. We found that the transits of faint-star TOIs are approximately 3.5 times deeper on average compared to the rest of the TOI process in order to compensate for the drop in the photometric precision caused by the increase in the limiting magnitude. Furthermore, luminous and therefore large stars are overrepresented in a magnitude-limited search, which also favors the detection of large planets. Second, we reviewed QLP results from the Primary Mission, for which most stars were observed in only a single 27.4 days sector. Given that multiple transits are needed to confirm periodicity, this baseline limits the majority of detectable signals to those with orbital periods less than half the length of a sector.

Compared to the rest of the Primary Mission TOI process, faint-star TOIs are fainter on average by 2.4 mag in the TESS band (Figure 3). Consequently, with an average distance to the solar system of 615 pc, faint-star TOI hosts are three times more distant than the rest of the TOIs. They are also preferentially hosted by large (Sunlike and larger) stars, with a larger radius by 10% on average. We expect that the absence

of M dwarfs will be addressed in our analysis of Extended Mission data (T. Daylan et al. 2022, in preparation) thanks to the change of the FFI cadence from 30 to 10 minutes, given the relatively small size of M dwarfs and correspondingly smaller transit durations of planets orbiting them.

3.2. Scientific Implications

Of the 1617 faint-star TOIs, 1014 (63%) can be considered hot Jupiter candidates ($R_p > 9 R_{\oplus}$, $P < 10$ days), nearly a factor of 10 more than the number of hot Jupiters found by the Kepler mission.¹⁴ While some of these TOIs will unavoidably be false positives (Santerne et al. 2013), these findings demonstrate TESS’s potential for significantly improving our understanding of hot Jupiter demographics. Yee et al. (2021) predicted that a faint magnitude-limited survey with TESS could increase the number of hot Jupiters over Kepler by an order of magnitude, and our faint-star search supports this prediction. Because the identification of planet candidates by our pipeline still relies on biased manual inspection, we caution that the hot Jupiters discovered by the faint-star (or regular TOI) process should not yet be used for statistical analysis. However, identification of TOIs early on gives the follow-up community time to statistically validate planets and identify false positives.

New TOIs are also promising targets for multiplanet searches, especially when TESS reobserves many of these stars in the current Extended Mission and beyond. The Kepler mission has shown that multiplanet systems are common (e.g., Yang et al. 2020), and the orbital planes of additional planets in known transiting planet systems are highly likely to be aligned with our line of sight. While rare, companions to hot Jupiters are also valuable probes of hot Jupiter formation. Our faint-star search has already uncovered a new TESS multiplanet system, TIC-352682207 (TOI-4010), a K dwarf which potentially hosts three close-in planets (M. Kunimoto et al. 2022, in preparation).

3.3. Promising Targets for Spectroscopic Follow-up

One of the primary goals of the TESS mission is to discover small planets ($R_p < 4 R_{\oplus}$) suitable for mass measurements via ground-based radial velocity (RV) observations (Ricker et al. 2014).

¹³ Accessed 2021 November 30 via ExoFOP (2019).

¹⁴ Based on the number of confirmed and candidate Kepler Objects of Interest listed on the NASA Exoplanet Archive (2019), accessed 2021 September 4.

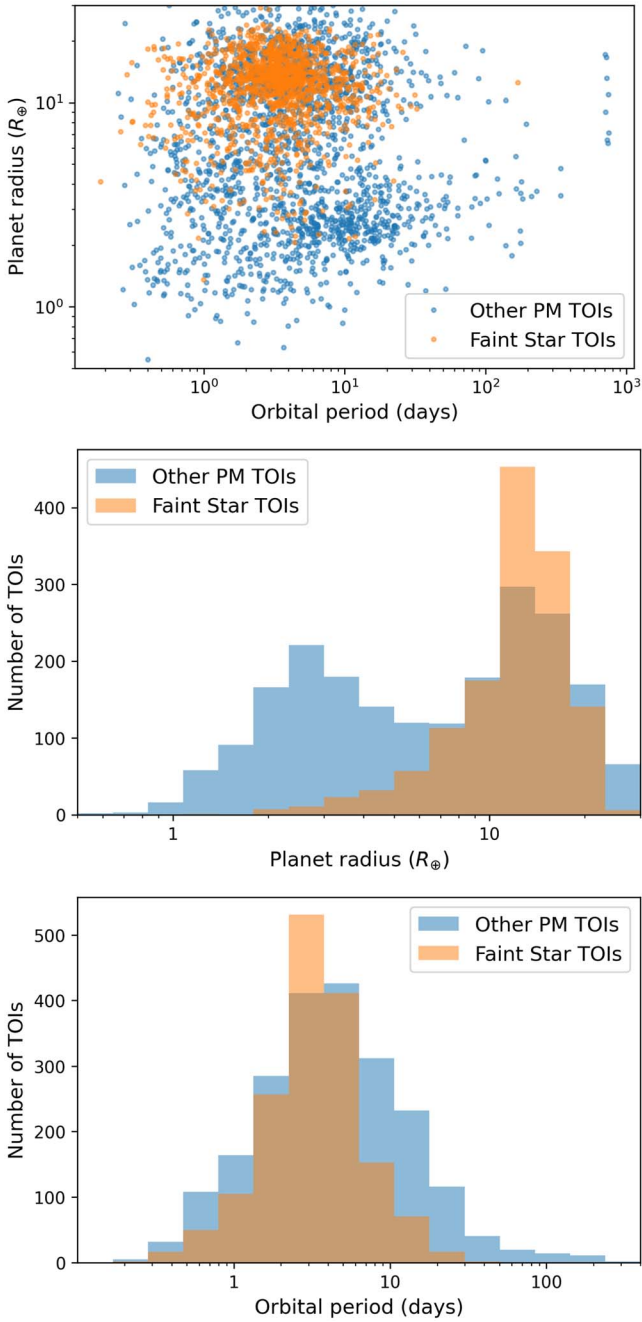


Figure 2. A comparison of TOI properties from the TOI catalog, with the faint-star TOIs in orange and other TOIs from the Primary Mission (Guerrero et al. 2021) in blue. Top: TOIs plotted in period–radius space. TOIs larger than $30 R_{\oplus}$ are not shown as they are highly unlikely to be planetary. Middle: histograms of planet radii. Bottom: histograms of orbital periods. The faint-star TOIs are predominantly giant candidates ($R_p > 10 R_{\oplus}$) and those with short orbital periods ($P < 10$ days).

To prioritize targets for RV follow-up, we estimate the predicted RV semiamplitude K for each small planet using

$$K = 28.4 \left(\frac{M_p}{M_J} \right) \left(\frac{M_p + M_s}{M_{\odot}} \right)^{-1/2} \left(\frac{a}{1 \text{ au}} \right)^{-1/2} \text{ m s}^{-1} \quad (1)$$

where M_J is a Jupiter mass, M_p is planet mass converted from R_p using the mass–radius relations from Chen & Kipping (2017), M_s is the stellar mass, and circular, edge-on orbits have been assumed.

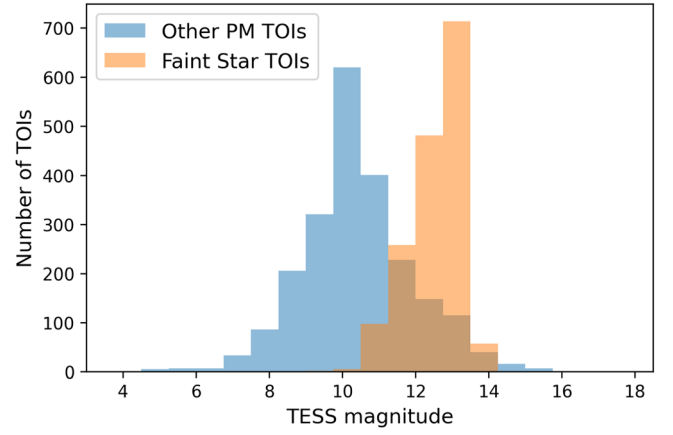


Figure 3. A comparison of the TESS magnitudes of TOI hosts, with the faint-star TOIs in orange and other TOIs from the Primary Mission in blue. On average, faint-star TOIs orbit stars 2.4 mag fainter than other Primary Mission TOIs.

Due to the nature of this work, the majority of our candidates are giants, or orbit stars too faint for RV follow-up. However, we find 10 planet candidates with $R_p < 4 R_{\oplus}$ and expected $K > 1 \text{ m s}^{-1}$ that orbit stars brighter than $V = 12$ mag. Of these, two (TOI-4110.01 and 4219.01) have $K > 5 \text{ m s}^{-1}$. We also find three small-planet candidates (TOI-2486.01, 2768.01, and 4010.03) with $K > 5 \text{ m s}^{-1}$ that orbit likely K and M dwarf stars brighter than $T = 12$ mag, which may be more accessible with spectrographs that operate in the red end of the spectrum (e.g., MAROON-X; Seifahrt et al. 2018). For those interested in the follow-up of larger planets, 99 of our planet candidates have $K > 10 \text{ m s}^{-1}$ and orbit stars brighter than $V = 12$ mag.

A secondary goal of TESS is to discover exoplanet targets amenable to atmospheric characterization. We adopted the framework developed by Kempton et al. (2018) to identify the most promising targets from our TOI list. Kempton et al. (2018) introduced the transmission spectroscopy metric (TSM) and emission spectroscopy metric (ESM), which quantify the expected S/N in transmission and thermal emission spectroscopy, respectively. Planet candidates satisfying $R_p < 4 R_{\oplus}$ and $\text{TSM} > 10$ or $R_p < 10 R_{\oplus}$ and $\text{TSM} > 90$ can be considered high-quality targets for transmission spectroscopy, while small planets with $R_p < 1.5 R_{\oplus}$ and $\text{ESM} > 7.5$ are good targets for emission spectroscopy (Kempton et al. 2018). We calculated the TSM and ESM for each of our planet candidates with $R_p < 10 R_{\oplus}$, and found 31 with $\text{TSM} > 90$.

One highlighted faint-star TOI is the small-planet candidate TOI-2486.01 ($R_p = 3.7 R_{\oplus}$, $P = 1.5$ days). TOI-2486.01 orbits a late K dwarf ($M_s = 0.66 M_{\odot}$, $R_s = 0.77 R_{\odot}$, $T_{\text{eff}} = 4205 \text{ K}$) which is one of our brighter targets in the TESS band ($T = 11.1$ mag). With both $K = 9.8 \text{ m s}^{-1}$ and $\text{TSM} = 92.4$, we consider this our best small candidate for spectroscopic follow-up. TOI-2486.01 was also independently detected by Montalto et al. (2020).

4. Concluding Remarks

We have described the identification of 1617 new TOIs hosted by stars brighter than $T = 13.5$ mag using FFIs collected in the TESS Primary Mission. These planet candidates were initially detected by the QLP at MIT, which performs multisector BLS transit searches for all stars with $T < 13.5$ mag, but limits nominal vetting efforts to planet-hosting stars brighter than $T = 10.5$ mag. Our vetting included an

independent and automated vetting pipeline, followed by manual review to determine the final list of TOIs to be alerted. Overall, the TOIs resulting from this work constitute roughly 40% of all TOIs from the TESS Primary Mission. With the identification of more than 1000 new hot Jupiter candidates, these faint-star TOIs will allow TESS to significantly improve understanding of giant, close-in exoplanets.

The vetting pipeline described in this work enabled the inspection of $\sim 700,000$ signals which would otherwise have to be manually reviewed by QLP operators. We plan to extend this pipeline further into a fully automated planet-vetting pipeline designed specifically for TESS by tuning our metric thresholds and adding new tests in the future. Aside from further reducing manual workload on vetting planet candidates, this will also apply to exoplanet occurrence rate studies, which require uniformly produced planet catalogs and accurately characterized selection functions.

Our review of lightcurves of faint stars from the TESS Extended Mission (Cycles 3 and 4) is ongoing and will be published in a future work.

We thank the referee for the constructive comments which greatly improved the manuscript. This paper utilizes data from the Quick-Look Pipeline (QLP) at the TESS Science Office (TSO) at MIT. The TESS mission is funded by NASA's Science Mission Directorate.

This research has made use of the Exoplanet Follow-up Observation Program website, which is operated by the California Institute of Technology, under contract with the National Aeronautics and Space Administration under the Exoplanet Exploration Program.

Software: `lmfit` (Newville et al. 2016), `matplotlib` (Hunter 2007), `numpy` (Harris et al. 2020), `scipy` (Virtanen et al. 2020), `tess-point` (Burke et al. 2020).

ORCID iDs

Michelle Kunimoto  <https://orcid.org/0000-0001-9269-8060>
 Tansu Daylan  <https://orcid.org/0000-0002-6939-9211>
 Natalia Guerrero  <https://orcid.org/0000-0002-5169-9427>
 William Fong  <https://orcid.org/0000-0003-0241-2757>
 Steve Bryson  <https://orcid.org/0000-0003-0081-1797>
 George R. Ricker  <https://orcid.org/0000-0003-2058-6662>
 Michael Fausnaugh  <https://orcid.org/0000-0002-9113-7162>

Chelsea X. Huang  <https://orcid.org/0000-0003-0918-7484>
 Lizhou Sha  <https://orcid.org/0000-0001-5401-8079>
 Avi Shporer  <https://orcid.org/0000-0002-1836-3120>
 Andrew Vanderburg  <https://orcid.org/0000-0001-7246-5438>
 Roland K. Vanderspek  <https://orcid.org/0000-0001-6763-6562>
 Liang Yu  <https://orcid.org/0000-0003-1667-5427>

References

- Bryson, S. T., Jenkins, J. M., Gilliland, R. L., et al. 2013, *PASP*, **125**, 889
 Burke, C. J., Levine, A., Fausnaugh, M., et al. 2020, TESS-Point: High precision TESS pointing tool, Astrophysics Source Code Library, ascl:2003.001
 Chen, J., & Kipping, D. 2017, *ApJ*, **834**, 17
 Claret, A. 2017, *A&A*, **600**, A30
 Coughlin, J. L. 2017, Description of the TCERT Vetting Reports for Data Release 25, Kepler Science Document, KSCI-19105-002, <https://ntrs.nasa.gov/citations/20170007765>
 Coughlin, J. L., Mullally, F., Thompson, S. E., et al. 2016, *ApJS*, **224**, 12
 ExoFOP 2019, Exoplanet Follow-up Observing Program—TESS (IPAC)
 Guerrero, N. M., Seager, S., Huang, C. X., et al. 2021, *ApJS*, **254**, 39
 Harris, C. R., Millman, K. J., van der Walt, S. J., et al. 2020, *Natur*, **585**, 357
 Hartman, J. D., & Bakos, G. Á. 2016, *A&C*, **17**, 1
 Huang, C. X., Vanderburg, A., Pál, A., et al. 2020, *RNAAS*, **4**, 204
 Hunter, J. D. 2007, *CSE*, **9**, 90
 Jenkins, J. M., Twicken, J. D., McCauliff, S., et al. 2016, *Proc. SPIE*, **9913**, 99133E
 Kempton, E. M. R., Bean, J. L., Louie, D. R., et al. 2018, *PASP*, **130**, 114401
 Kostov, V. B., Mullally, S. E., Quintana, E. V., et al. 2019, *AJ*, **157**, 124
 Kovács, G., Zucker, S., & Mazeh, T. 2002, *A&A*, **391**, 369
 Kunimoto, M., Huang, C., Tey, E., et al. 2021, *RNAAS*, **5**, 234
 Mandel, K., & Agol, E. 2002, *ApJL*, **580**, L171
 Montalto, M., Borsato, L., Granata, V., et al. 2020, *MNRAS*, **498**, 1726
 NASA Exoplanet Archive 2019, Kepler Objects of Interest Cumulative Table (IPAC)
 Newville, M., Stensitzki, T., Allen, D. B., et al. 2016, Lmfit: Non-Linear Least-Square Minimization and Curve-Fitting for Python, Zenodo, doi: [10.5281/zenodo.11813](https://doi.org/10.5281/zenodo.11813)
 Ricker, G. R., Winn, J. N., Vanderspek, R., et al. 2014, *Proc. SPIE*, **9143**, 914320
 Santerne, A., Díaz, R. F., Almenara, J. M., et al. 2013, in SF2A-2013: Proc. Annual Meeting of the French Society of Astronomy and Astrophysics, ed. L. Cambresy et al., **555**
 Seifahrt, A., Stürmer, J., Bean, J. L., & Schwab, C. 2018, *Proc. SPIE*, **10702**, 107026D
 Stassun, K. G., Oelkers, R. J., Paegert, M., et al. 2019, *AJ*, **158**, 138
 Thompson, S. E., Coughlin, J. L., Hoffman, K., et al. 2018, *ApJS*, **235**, 38
 Virtanen, P., Gommers, R., Oliphant, T. E., et al. 2020, *NatMe*, **17**, 261
 Yang, J.-Y., Xie, J.-W., & Zhou, J.-L. 2020, *AJ*, **159**, 164
 Yee, S. W., Winn, J. N., & Hartman, J. D. 2021, *AJ*, **162**, 240
 Yu, L., Vanderburg, A., Huang, C. X., et al. 2019, *AJ*, **158**, 25